Article

Cell Chemical Biology

Enzyme-Dependent [4 + 2] Cycloaddition Depends on Lid-like Interaction of the N-Terminal Sequence with the Catalytic Core in PyrI4

Graphical Abstract

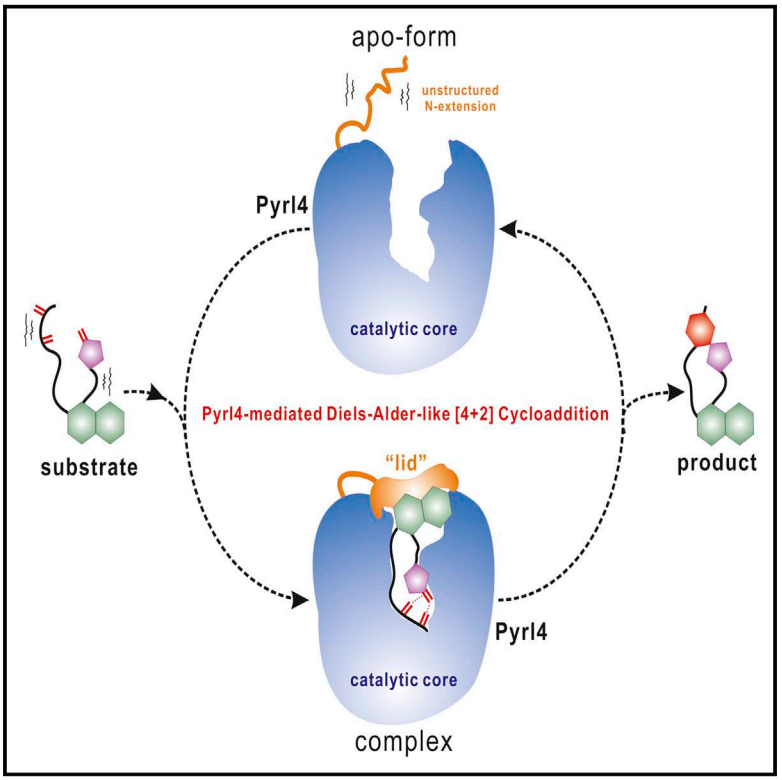

Highlights

- PyrI4 is a dedicated β barrel protein catalyzing a [4 + 2] cycloaddition reaction
- The cyclization results from a synergistic conformational constraint in the β barrel
- The cyclization relies on the ligand-binding-inducible *N*-terminal sequence of PyrI4
- PyrI4 behaves in a highly dynamic, lid-like trapping manner to cycle its reaction

Authors

Qingfei Zheng, Yujiao Guo, Linlin Yang, ..., Hualiang Jiang, Lifeng Pan, Wen Liu

Correspondence

panlf@sioc.ac.cn (L.P.), wliu@mail.sioc.ac.cn (W.L.)

In Brief

Zheng et al. discovered that the β barrel protein PyrI4 appears to behave in a highly dynamic, lid-like trapping manner to establish the rigid pentacyclic scaffold of the spirotetramate antibiotics pyrroindomycins, providing an extraordinary paradigm for understanding how nature cycles a completely enzyme-dependent [4 + 2] cycloaddition reaction.

Accession Numbers

5BTU
5BU3

Zheng et al., 2016, Cell Chemical Biology *23*, 352–360
March 17, 2016
http://dx.doi.org/10.1016/j.chembiol.2016.01.005

Please cite this article as: Zheng et al., Enzyme-Dependent [4 + 2] Cycloaddition Depends on Lid-like Interaction of the N-Terminal Sequence with the Catalytic Core in Pyrl4, Cell Chemical Biology (2016), http://dx.doi.org/10.1016/j.chembiol.2016.01.005

Enzyme-Dependent [4 + 2] Cycloaddition Depends on Lid-like Interaction of the N-Terminal Sequence with the Catalytic Core in Pyrl4

Qingfei Zheng,[1,4] Yujiao Guo,[1,4] Linlin Yang,[2] Zhixiong Zhao,[1] Zhuhua Wu,[1] Hua Zhang,[1] Jianping Liu,[1] Xiaofang Cheng,[1] Jiequn Wu,[1,3] Huaiyu Yang,[2] Hualiang Jiang,[2] Lifeng Pan,[1,*] and Wen Liu[1,3,*]

[1]State Key Laboratory of Bioorganic and Natural Products Chemistry, Shanghai Institute of Organic Chemistry, Chinese Academy of Sciences, 345 Lingling Road, Shanghai 200032, China

[2]Drug Discovery and Design Center, State Key Laboratory of Drug Research, Shanghai Institute of Materia Medica, Chinese Academy of Sciences, 555 Zu-Chong-Zhi Road, Shanghai 201203, China

[3]Huzhou Center of Bio-Synthetic Innovation, 1366 Hongfeng Road, Huzhou 313000, China

[4]Co-first author

*Correspondence: panlf@sioc.ac.cn (L.P.), wliu@mail.sioc.ac.cn (W.L.)

http://dx.doi.org/10.1016/j.chembiol.2016.01.005

SUMMARY

The Diels-Alder [4 + 2] cycloaddition reaction is one of the most powerful and elegant organic synthesis methods for forming 6-membered molecules and has been known for nearly a century. However, whether and how enzymes catalyze this type of reaction is still not completely clear. Here we focus on Pyrl4, an enzyme found in the biosynthetic pathway of pyrroindomycins where it catalyzes the formation of a spiro-conjugate via an enzyme-dependent *exo*-selective [4 + 2] cycloaddition reaction. We report the crystal structures of Pyrl4 alone and in complex with its product. Comparative analysis of these structures, combined with biochemical analysis, lead us to propose a unique trapping mechanism whereby the lid-like action of the N-terminal tail imposes conformational constraints on the β barrel catalytic core, which enhances the proximity and polarization effects of reactive groups (1,3-diene and alkene) to drive cyclization in a regio- and stereospecific manner. This work represents an important step toward the wider application of enzyme-catalyzed [4 + 2] cyclization for synthetic purposes.

INTRODUCTION

The pyrroindomycins (PYRs, Figure 1) are spirotetramate natural products; they were isolated from *Streptomyces rugosporus* during the screening of agents active against drug-resistant bacterial pathogens, such as methicillin-resistant *Staphylococcus aureus* and vancomycin-resistant *Enterococcus faecium* (Ding et al., 1994; Singh et al., 1994). These molecules possess a characteristic aglycone that contains two cyclohexene units present in both the dialkyldecalin and the tetramate spiro-conjugate portions. We recently elucidated the biosynthetic pathway of PYRs and showed that a modular polyketide synthase-nonribosomal peptide synthetase hybrid system programs the assembly of a tetramate-containing linear intermediate, which features two pairs of 1,3-diene and alkene groups as the structural hallmarks of a [4 + 2] cycloaddition cascade (Pang et al., 2016; Tian et al., 2015; Wu et al., 2012). Consistently, two dedicated cyclases in tandem catalyze the formation of two cyclohexene rings (Figure 1): PyrE3, a FAD-dependent enzyme involved in dialkyldecalin formation, generates the partially cyclized intermediate **1**; and Pyrl4 then acts as a spiro-conjugate synthase to complete the pentacyclic core (**2**; Tian et al., 2015). This unusual cross-bridging strategy is common for the biosynthesis of spirotetronates, e.g., chlorothricin (Jia et al., 2006; Tian et al., 2015) and versipelostatin (Hashimoto et al., 2015), the natural products structurally related to PYRs and sharing a similar pentacyclic aglycone that differs in size, substitution pattern, and composition of the five-membered heterocyclic moiety (Lacoske and Theodorakis, 2015).

Enzymes previously known to have [4 + 2] cycloaddition activity are remarkably few, typically displaying multiple functions, lacking catalytic efficiency, or participating in reactions that proceed spontaneously (Oikawa and Tokiwano, 2004; Klas et al., 2015; Kim et al., 2012; Pang et al., 2016; Zheng et al., 2016). In contrast, the newly identified dialkyldecalin synthases and spiro-conjugate synthases are monofunctional and effectively catalyze the completely enzyme-dependent reactions in a regio- and stereo-selective manner (Hashimoto et al., 2015; Tian et al., 2015), thereby providing ideal candidates for a detailed mechanistic examination of the existence of a bona fide Diels-Alderase, which catalyzes cyclohexene formation using the substrates 1,3-diene and alkene through a pericyclic transition state (Hashimoto et al., 2015; Tian et al., 2015). In this study, we provide structural insights into the spiro-conjugate synthase Pyrl4, with a focus on how this enzyme interacts with its ligand to catalyze an *exo*-selective [4 + 2] cycloaddition reaction.

RESULTS

Crystallization of Pyrl4

We determined the crystal structure of Pyrl4 in full length (residues 1–184) to 2.5-Å resolution (Figure 2A and Table S1).

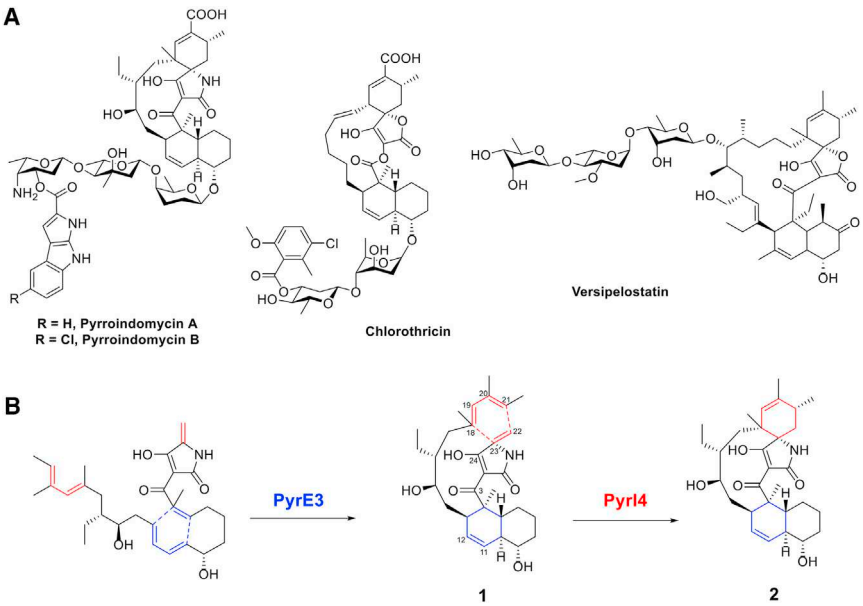

Figure 1. Chemical Structures and Biosynthetic Route

(A) The spirotetramates pyrroindomycins (PYRs) A and B, and the spirotetronates chlorothricin and versipelostatin.

(B) Conversion of the linear intermediate that contains two pairs of 1,3-diene and alkene groups into the pentacyclic core in the PYR biosynthetic pathway. PyrE3-catalyzed dialkyldecalin formation is indicated in blue, and PyrI4-catalyzed spiro-conjugate formation is highlighted in red.

Consistent with the observation in solution (Figure S1), analysis of the PyrI4 crystal structure revealed that two protein units pack perpendicularly to each other to form a unique symmetrical dimer (Figure 2A). Each unit features a β barrel core, composed of nine β strands (β1–β9) and a short α helix (α3) located between β6 and β7 to create a solvent-exposed, highly acidic pocket (Figures 2A–2D). The N-terminal 22 amino acid (aa) residues of PyrI4 were not modeled due to a lack of electron density. Using nuclear magnetic resonance (NMR) spectroscopy, we traced these residues and confirmed that they constitute an unstructured sequence based on analysis of the $^{13}C_{\alpha}$ and $^{13}C_{\beta}$ chemical shifts (Figure S2). Two α helixes (α1 and α2) are located between this sequence and the β barrel core. The α1 helix is important for dimer formation, as a ~1,351-Å^2 interface area of the two units mainly attributes to its extensive interaction (either hydrophobic or polar) with the β barrel core of the counterpart (Figures 2A and 2B and Figures S3A–S3C). The structural similarity survey based on the β barrel structure of PyrI4 revealed only a few homologs. Intriguingly, one of them is PpAOC2 (PDB: 4H6A; Neumann et al., 2012), the allene oxide cyclase in the biosynthetic pathway of oxylipins, and this trimeric enzyme was assumed to catalyze a pericyclic reaction for *cis*(+)-oxo-phytodienoate formation (Figure S4). Overall, the architecture of PyrI4 is rigid, consistent with its extreme stability in in vitro assays, e.g., it retained over 50% of the activity after being boiled at 100°C for 20 min (Figure 4C).

Crystallization of PyrI4 in Complex with Product 2

We determined the co-crystal structure of PyrI4 in complex with the ligand to 1.9-Å resolution (Figure 2E and Table S1). The crystallization that was initially conducted using PyrI4 and substrate **1** resulted in a dimeric complex of PyrI4 with product **2** (in 1:1 stoichiometry) due to complete conversion. In contrast, extensive efforts to crystallize or soak product **2** directly into crystals under various conditions were unsuccessful. In the complex structure (Figures 2E–2G), product **2** is tightly encapsulated in the β barrel, with an orientation directed by the insertion of the spiro-conjugate portion deeply into the highly acidic cavity and the exposure of the dialkyldecalin system to the solvent phase. Specifically, the hydrophobic skeleton of **2** packs extensively with the hydrophobic patch formed by residues A10, A13, A67, L70, V72, T81, V83, Y85, V106, M109, M113, I134, C136, M139, L140, and L165, and its polar groups interact with Q115 (described below) and with R9, A10, C136, and Y177 via several water-mediated hydrogen bonds (Figure 4A). Compared with the apo-form structure, the complex structure of PyrI4 exhibits little rearrangement in the β barrel core (Figure S3D). Based on the conformation of product **2** in the complex, modeling of substrate **1** into PyrI4 resulted in a conformer of **1**, which is compatible with the *exo* transition state structure of an asynchronous Diels-Alder reaction (Figure 3), thereby indicating the feasibility that PyrI4 accommodates the 1,3-diene and alkene groups in the cavity of the β barrel for a regio- and stereo-selective pericyclic reaction.

Mutagenesis-Based Bioassays of the Enzymatic Activity

The key residue Q115 of PyrI4 within a ~644-Å^2 interface area was identified due to its specific polar interactions with the hydroxyl at C24 and the carbonyl at C3 of the ligand via two hydrogen bonds (Figure 4A). These interactions provide an electron-withdrawing effect on the substrate, which might lower the lowest unoccupied molecular orbital (LUMO) energy of the dienophile to accelerate the [4 + 2] cycloaddition. Indeed, the substitution of Q115 with Ala resulted in a ~60% loss of enzymatic activity at constant temperature (Figure 4C). Centering on the acidic cavity of the β barrel surrounding the 1,3-diene-derived portion of the ligand, we selectively mutated the residues that are acidic (E65A and E87A), sterically closed (Y85A and H117A), and involved in hydrophobic interactions (I134A and M139A) and water-mediated hydrogen bonding (Y177A). Each mutation caused a ~5%–30% decrease in enzymatic activity (Figure 4C), primarily by lowering the catalytic rate, but introduced only a slight change in substrate-binding ability as assessed by selective kinetic analysis (Table S2). Consequently, a synergistic conformation constraint in the rigid β barrel structure of PyrI4 plays a crucial role in the conversion of **1** to **2**, as multiple mutations of these residues, Q115A/Y85A, Q115A/Y85A/E65A, Q115A/Y85A/E65A/E87A, Y85A/E65A/E87A, and Y85A/E65A/E87A/Y177A, showed additive effects toward the

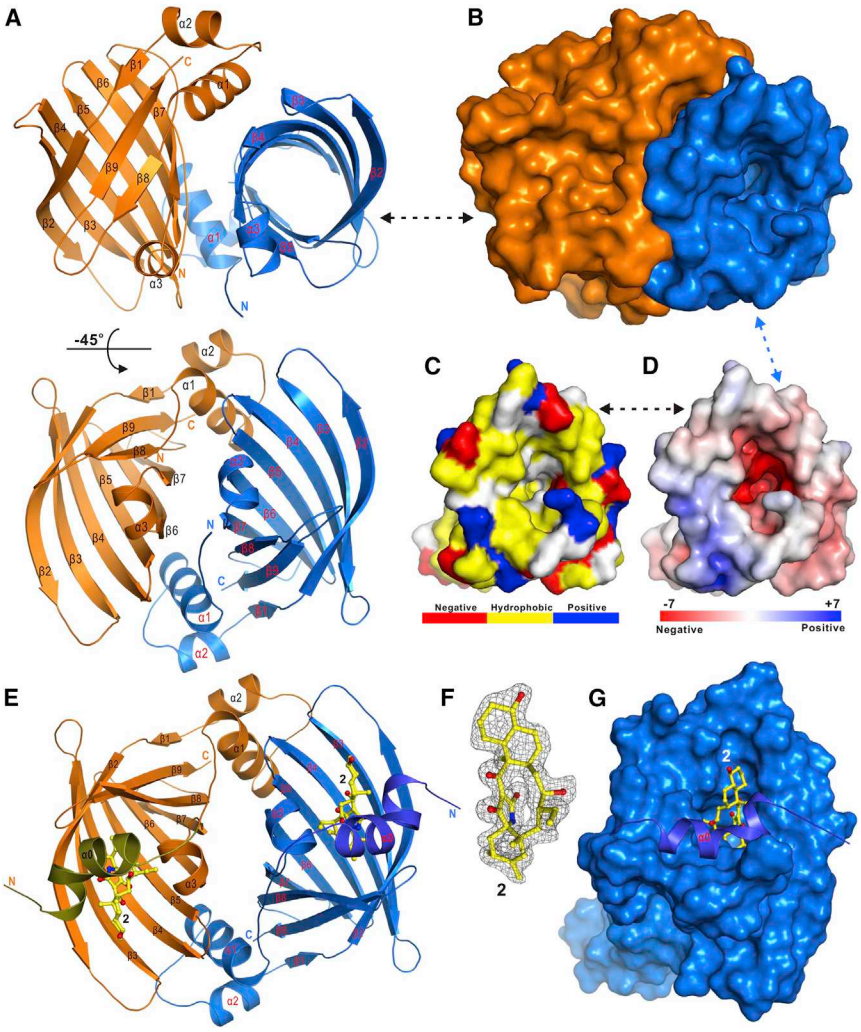

Figure 2. Structures of PyrI4 alone and Its complex with 2

(A and B) Ribbon diagram and surface representation showing the dimer architecture.

(C) Surface representation showing the solvent-exposed pocket. The residues that are hydrophobic or polar (positively or negatively charged and uncharged) are indicated in color.

(D) Surface charge potential representation (contoured at ±7 kT/eV; blue/red) showing the highly acidic cavity.

(E) Combination of the ribbon representation (for the protein) and the stick-ball model (for the ligand) showing the complex structure. The protein is colored as in (A), with the exception of the structured N-terminal sequence (residues 1–22), which is highlighted in a different color.

(F) $F_o - F_c$ map of product **2** showing that the electron density can be clearly assigned. The map is calculated by omitting **2** from the final PDB file and contoured at 2.5σ.

(G) Combination of the surface representation and the ribbon-stick model showing that product **2** is tightly encapsulated in the pocket of β barrel by the N-terminal sequences. The core structure of the protein, lid-like N-terminal sequences and product **2** are shown in surface representation, ribbon diagram, and stick model, respectively.

nearly complete inactivation of the enzyme (Figure 4C). The acidic pocket of the β barrel provides an internal environment that may facilitate negative charge removal from the tetramate moiety of **1** (Yamaguchi et al., 1976) to lower the LUMO energy of dienophile, thereby allowing the Diels-Alder-like cyclization to proceed under the condition of physiological pH.

Necessity of the Structurally Variable N-Terminal Sequence

Comparative analysis of the two PyrI4 structures revealed a remarkable difference, as the initially disordered 22-aa N terminus of its apo-form has been structured to form the sequence containing a highly bent α helix (α0) in the complex with product **2** (Figures 2A and 2E). The α0 helix buries the ligand in the β barrel by stacking on the concave rim composed of the strands β2, β8 and β9, and the α3-helix (Figures 2E and 2G). To tightly lock the ligand, the interaction between α0 and the β barrel includes extensive hydrophobic contacts (e.g., I6 and A10 contact a groove formed by A67, L70, and P174) and particularly three salt bridges from residues R9, E12, and E20 to residues D74, R173, and R141, respectively (Figure 4B). There is a strong hydrogen bond between A17 and R142 that further stabilizes the configuration of α0. To validate the necessity of this α helix, we deleted the N-terminal 10-aa residues of PyrI4. Although the destruction of α0 had only a slight effect on the overall structure of PyrI4, as indicated by the high similarity between the PyrI4-Δ10 variant and the full-length protein in the ^{1}H-^{15}N heteronuclear single quantum coherence (HSQC) spectrum (Figure 5A), the associated conversion of **1** to **2** was completely abolished (Figures 4C and S5). We then introduced the site-specific mutations E20R, D74R, and R9A to weaken the interaction between α0 and the β barrel by destroying one of the three salt bridges. As anticipated, each mutation exclusively inactivated the enzyme (Figure 4C). Therefore, the ligand-mediated interaction of α0 with the β barrel is indispensable for the reaction to proceed, and the substrate-induced formation of multiple salt bridges and hydrogen bonds may release the affinity energy of PyrI4 and **1**, thereby overcoming the unfavorable entropy-decrease cyclization process through the enthalpy effect.

Dynamic Analysis of the N-Terminal Sequence by NMR Spectroscopy

To examine the dynamic nature of the 22-aa N-terminal sequence of PyrI4, we titrated the ^{15}N-labeled protein with the ligand in solution. NMR analysis revealed that titration using **1** or **2** largely changed the signals corresponding to the 22-aa N-terminal sequence, particularly residues E8, R9, Q19, and E20 (Figures 5B and S6). The change appeared in a ligand dose-dependent manner, as judged by the associated signal intensity and

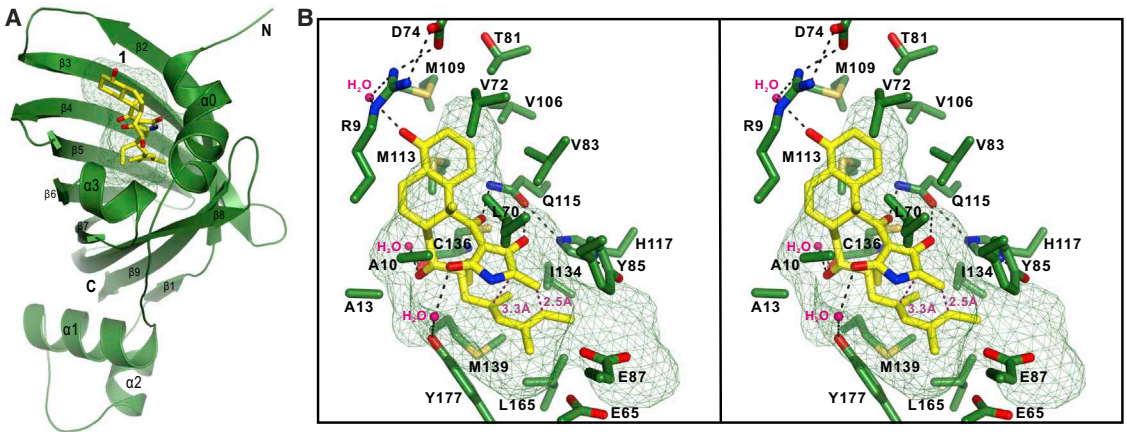

Figure 3. Docking Model of PyrI4 in Complex with Substrate 1

(A) Combination of the ribbon-surface representation and the stick model showing the overall docking structure. Substrate **1** shown in the stick model deeply binds to the pocket of PyrI4, which is shown in the ribbon-surface (pocket only) model.

(B) Stereo view showing the detailed interactions between PyrI4 and substrate **1**. The hydrogen bonds involved in the binding are shown as dotted lines. PyrI4 accommodates **1** in a highly folded conformation, leading to approaching of the alkene group to the *cis*-1,3-diene group. For carbon-carbon bond formation, the distance between C21 and C22 (2.5 Å) is much shorter than that of C18 and C23 (3.3 Å), consistent with our theoretical calculation results.

chemical shift in the ^{1}H-^{15}N HSQC spectrum, indicating that there is a specific interaction required for molecular recognition between the ligand and the sequence. This interaction could induce the formation of the α0 helix arising from the 22-aa N-terminal sequence of PyrI4, allowing the substrate to become locked within the β barrel catalytic core. However, the trapping process tends to specifically proceed on the partially cyclized substrate **1**, which is more flexible than the highly rigidified product **2**. This preference may account for the aforementioned failure in direct complex crystallization using PyrI4 and **2**. After conversion, the conformational change of **2** from the highly folded form, as observed in the crystal complex with PyrI4 (Figure 2F), to the stable form in solution may provide a sufficient amount of energy to break the interaction between the lid-like N-terminal sequence and the β barrel catalytic core, thus avoiding potential product inhibition and releasing the product to cycle the reaction.

DISCUSSION

Diels-Alder-type [4 + 2] cycloaddition represents one of the most important reactions for carbon-carbon bond formation. Relevant synthetic methodology development has been the subject of considerable effort in view of its central role in the theory and practice of organic chemistry (Du and Ding, 2010). This transformation has long been envisioned to be present in the biosynthesis of a number of cyclohexene-containing natural products (Kim et al., 2012). However, the process through which nature works remains elusive, leaving the question of whether a Diels-Alderase occurs naturally unsolved for decades.

Here we demonstrated that PyrI4 catalyzes spiro-conjugate formation through unique interactions with the ligands (substrate and product) in the biosynthetic pathway of PYRs, the spirotetramate antibiotics. The combined structural and biochemical evidence is consistent with the hypothesis that this enzyme functions as an *exo*-selective Diels-Alderase, although validation of the associated reaction through a pericyclic transition state needs further proof, by (1) trapping the flexible substrate with the dynamic N-terminally extended sequence, (2) synergistically constraining its conformation to an *exo* transition state structure in the rigid β barrel core, (3) accelerating the reaction through an electron-withdrawing effect on dienophile, and finally, (4) releasing the rigidified product and avoiding its inhibition effect for cycling on the change in chemical conformation.

With a resemblance to various artificially developed Diels-Alderases (Gouverneur et al., 1993; Seelig and Jäschke, 1999; Siegel et al., 2010), PyrI4 could stabilize the transition state by regio- and stereo-selectively accommodating the 1,3-diene and alkene groups of the substrate; however, to overcome this unfavorable entropy-decrease process relies on the enthalpy effect arising from the interaction among its N-terminal sequence, the β barrel core, and the substrate. Similar to SpnF, another structurally characterized Diels-Alder-like [4 + 2] cyclase in the biosynthesis of spinosyn A (Kim et al., 2011; Fage et al., 2015), PyrI4 appears to have no absolutely critical catalytic amino acids. Instead, nature seemly utilizes different protein architectures to fit unrelated substrates and conduct this type of reaction through a synergistic conformation constraint, as exemplified by the β barrel core of PyrI4 and VstJ, Rossmann fold with bound FAD for PyrE3 (Tian et al., 2015), and class I methyltransferase fold with bound *S*-adenosylhomocysteine for SpnF (Fage et al., 2015). Surprisingly, the N-terminal sequence of PyrI4 acts in a ligand-inducible manner, by formation or dissolution of a locking α helix according to the structural nature of the ligand (either the flexible substrate or rigidified product). Structural-based sequence alignment revealed that some homologs of PyrI4 (e.g., ChlL; Tian et al., 2015) are highly variable in the N-terminal sequence in contrast to the relatively conserved β barrel core (Figure 6), indicating that their interactions with ligands are specific and structure dependent. However, some homologs (e.g., VstJ; Hashimoto et al., 2015) apparently lack this N-terminal sequence, suggesting that there are different trapping strategies to achieve a similar [4 + 2] cycloaddition.

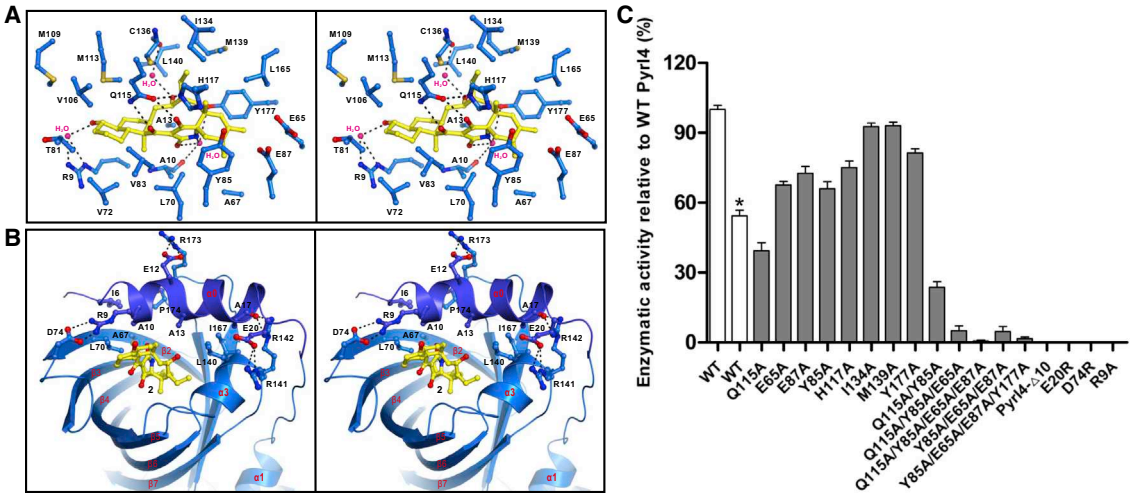

Figure 4. Identification and Characterization of the Residues of PyrI4 Involved in the Enzymatic Cycloaddition

(A) Stereo view showing the detailed interactions between PyrI4 and product **2**. The dotted lines indicate the associated hydrogen bonds.

(B) Stereo view showing the detailed binding interface between the β barrel core and the lid-like N-terminal sequences. The dotted lines indicate the associated salt bridges and hydrogen bonds.

(C) Comparison of the enzymatic activities of PyrI4 (white columns) and its variants (gray columns) at 30°C. The asterisk indicates that the reaction proceeded in the presence of the enzyme pre-treated by heating at 100°C for 20 min. The error bars represent the standard deviation from three different experiments. For selective kinetic analysis, see Table S2.

SIGNIFICANCE

The crystal structures of the dedicated spiro-conjugate synthase PyrI4 and in complex with its product are now available, along with NMR spectroscopy-associated analyses and mutagenesis-based biochemical assays. This rigid β barrel protein appears to behave in a highly dynamic, lid-like trapping manner to establish the pentacyclic scaffold of the spirotetramates PYRs, thereby providing an extraordinary paradigm for understanding how nature cycles a completely enzyme-dependent [4 + 2] cycloaddition reaction. The complementarity between the active-site structure of PyrI4 and the *exo*-selective transition state of the substrate arising from their non-covalent interactions could play a primary role in the cyclization reaction, the occurrence of which, however, relies on a synergistic conformational constraint motivated by the formation of an N-terminal locking α helix. The resulting proximity and polarization effects of reactive groups (1,3-diene and alkene) would dominate the regio- and stereo-selectivity of the product as well as accelerate the transformation rate. After the conversion, the effect of product inhibition, which is often encountered during the artificial design of biological Diels-Alder catalysts, could be avoided through the conformational change of the product from the highly folded form to the stable form in solution, to break the interaction between the lid-like N-terminal sequence and the β barrel catalytic core for product release. The structure-based dissection of the PyrI4-catalyzed [4 + 2] cyclization process represents a key step toward understanding, developing, and utilizing nature's strategy for the application of the Diels-Alder reaction in organic chemistry.

EXPERIMENTAL PROCEDURES

General Materials and Methods

Biochemical reagents and media were purchased from Sinopharm Chemical Reagent Company, Oxoid, or Sigma-Aldrich unless otherwise stated. Restriction endonucleases were purchased from Thermo Fisher Scientific. Chemical reagents were purchased from standard commercial sources.

DNA isolation and manipulation in *Escherichia coli* strains were performed according to standard procedures (Green and Sambrook, 2012). PCR amplifications were performed on an Applied Biosystems Veriti Thermal Cycler using either Taq DNA polymerase (Vazyme Biotech) for routine genotype verification or Phanta Max Super-Fidelity DNA Polymerase (Vazyme Biotech) for high-fidelity amplification. The synthesis of primers was performed at Shanghai Sangon Biotech. DNA sequencing was performed at Shanghai Majorbio Biotech or Shenzhen BGI in China.

High-performance liquid chromatography (HPLC) analysis was conducted on an Agilent 1200 HPLC system (Agilent Technologies). HPLC electrospray ionization mass spectrometry (HPLC-ESI-MS) analysis was performed on a Thermo Fisher LTQ Fleet ESI-MS spectrometer (Thermo Fisher Scientific). The data were analyzed using Thermo Xcalibur software.

Protein Expression and Purification

Briefly, the preparation of the native PyrI4 protein and its variants was performed according to procedures described previously (Tian et al., 2015), following expression in *E. coli* BL21 (DE3) at 16°C and disruption of the resulting cells using a low-temperature ultra-high-pressure cell disrupter (FB-110X, Shanghai Litu Machinery Equipment Engineering). Thrombin protease (Sigma-Aldrich) was used to remove the N-terminal tags. After further purification using size-exclusion chromatography, the recombinant proteins were analyzed by SDS-PAGE, and concentrated and desalted using a PD-10 Desalting Column (GE Healthcare) according to the manufacturer's protocols. The concentration of each protein was determined by the Bradford assay using BSA as the standard.

To prepare the SeMet-labeled protein, the cells were cultured in 1 l of M9 minimal medium (Green and Sambrook, 2012) at 37°C until they reached an $OD_{600\ nm}$ of 0.5. After supplementation with 0.06 g of SeMet (J&K Scientific), 0.1 g of lysine, threonine, and phenylalanine, and 0.5 g of leucine, isoleucine, and valine, protein expression was induced by the addition of

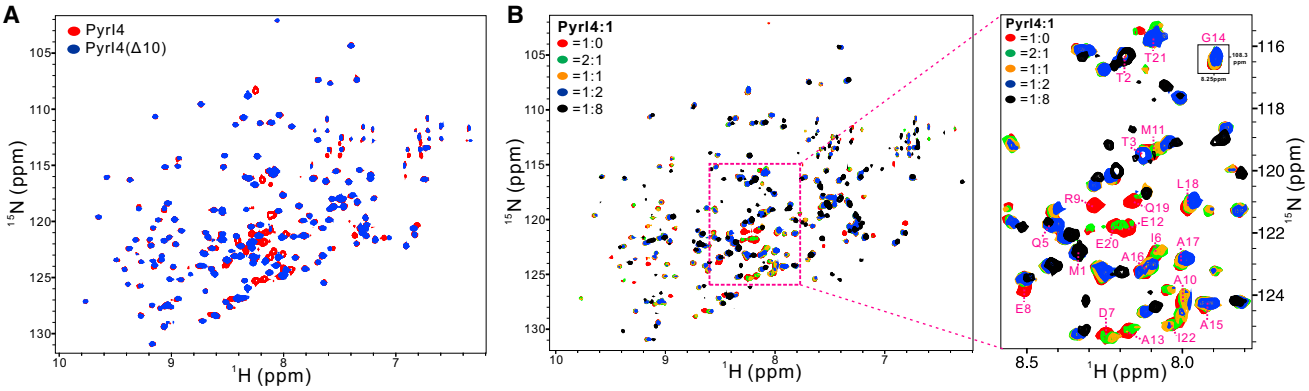

Figure 5. Analysis of the Pyrl4 Proteins in Solution by NMR

(A) Overlay plot of the ^{1}H-^{15}N HSQC spectra of Pyrl4 (red) and Pyrl4-Δ10 (blue).

(B) Superposition plot of the ^{1}H-^{15}N HSQC spectra of Pyrl4 in the titration with variable molar ratios of substrate **1**. For clarity, the right panel shows the enlarged view of a selected portion including all the signals for the NMR-observable residues of the flexible N-terminal sequence (residues 1–22), for which the chemical shift assignments are further labeled.

isopropyl-β-D-thiogalactopyranoside to a final concentration of 1 mM, followed by further incubation at 16°C overnight.

To prepare the ^{15}N- or ^{15}N,^{13}C-labeled proteins, the recombinant *E. coli* strains were cultured in M9 minimal medium that contained $^{13}C_6$-glucose and/or $^{15}NH_4Cl$ (Cambridge Isotope Laboratories) as the sole carbon and/or nitrogen sources.

For site-specific mutagenesis of Pyrl4, rolling-circle PCR amplification (using the primers listed in Table S4) followed by subsequent *Dpn*I digestion was performed according to the standard procedure of the QuickChange Site-Directed Mutagenesis Kit purchased from Stratagene (GE Healthcare) or Mut Express II (Vazyme Biotech). Each mutation was confirmed by sequencing.

Protein Crystallization and Structural Elucidation

Crystallization of the SeMet-Pyrl4 and Pyrl4-**2** complex was performed using the sitting-drop, vapor-diffusion method at 16°C. To obtain SeMet-Pyrl4 crystals, the solution composed of the SeMet-Pyrl4 protein (20 mg/ml in 20 mM Tris-HCl [pH 7.5]), 100 mM NaCl, 1 mM DTT, and 1 mM EDTA was mixed with an equal volume of reservoir solution containing Tris-HCl (100 mM [pH 6.5]) and polyethylene glycol monomethyl 1000 (20%, v/v). Prior to the diffraction experiments, glycerol (10%) was added as the cryo-protectant. For the Pyrl4-**2** complex, native Pyrl4 was saturated with substrate **1** (with a molar ratio up to 10:1 of **1** to Pyrl4). Crystals of the Pyrl4-**2** complex were harvested under the crystallization condition with 0.04 M citric acid, 0.06 M Bis-Tris propane (pH 6.4), and 20% w/v polyethylene glycol 3350. Prior to the diffraction experiments, the crystals were soaked in crystallization solution containing 1 mM **1** and 15% glycerol for cryo-protection.

All diffraction datasets were collected at the Shanghai Synchrotron Radiation Facility, and processed and scaled using HKL2000 (Table S1; Otwinowski and Minor, 1997). The single-wavelength anomalous diffraction phase was determined for the SeMet derivative dataset and a partial structural model was traced in AutoSol (Terwilliger et al., 2009). The structure model was built manually based on the experimental phase and then refined using PHENIX (Adams et al., 2002). COOT was used for model rebuilding and adjustments (Emsley and Cowtan, 2004). In the final stage, an additional TLS refinement was performed in PHENIX. The phase problem of the complex was solved by the molecular replacement method using the structure of the SeMet-Pyrl4 protein with PHASER (Storoni et al., 2004). The initial model was rebuilt manually and then refined using REFMAC (Murshudov et al., 1997). Further manual model building and adjustment were completed using COOT. The qualities of the final model were validated by MolProbity (Davis et al., 2007). The final refinement statistics are listed in Table S1. Structural diagrams were prepared using the program PyMOL (http://www.pymol.org/).

Determination of the Dimeric Nature of Pyrl4 in Solution

For the chemical cross-linking assay, the purified Pyrl4 (0.1 mM in 50 mM potassium phosphate buffer containing 50 mM NaCl, 1 mM DTT, and 1 mM EDTA at pH 6.5) alone or in combination with different concentrations of disuccinimidyl glutarate (0.1 mM, 0.4 mM, 1 mM, or 2 mM) was incubated at room temperature for 30 min before the reaction was quenched by the addition of 1 M Tris-HCl (pH 7.5). Then, the samples were analyzed by SDS-PAGE.

For multi-angle light-scattering measurement, the Pyrl4 sample (100 μl at a concentration of 20 μM) was injected into an AKTA FPLC system with a Superose 12 10/300 GL column (GE Healthcare) with column buffer containing 50 mM Tris-HCl, 100 mM NaCl, 1 mM DTT, and 1 mM EDTA at pH 7.8. The chromatography system was coupled to a static light-scattering detector (miniDawn, Wyatt Technology) and a differential refractive index detector (Optilab, Wyatt Technology). Data were collected every 0.5 s with a flow rate of 0.2 ml/min. Data were analyzed using ASTRA 6 (Wyatt Technology).

Enzymatic Activity Assays and Kinetic Analysis

For activity related to the native protein, assays were conducted at 30°C in a mixture containing 1 mM compound **1** in 50 mM Tris-HCl buffer (pH 7.0). Pyrl4 or its variant was added to the solution at a final concentration of 40 μM to initiate the reaction (the total volume was 100 μl). After 1 min of incubation, during which the production of **2** was linear with respect to time (Tian et al., 2015), the reaction was quenched by adding a 2-fold volume of methanol. The reaction proceeding in the absence of the enzyme was used as a negative control. To test the stability of Pyrl4, the intact native enzyme was boiled for 20 min at 100°C before adding to the reaction mixture. HPLC-MS analysis of the conversion was performed according to the method described previously (Tian et al., 2015). All assays were performed in triplicate.

Kinetic analysis was conducted according to the procedures described previously (Tian et al., 2015). Briefly, the enzymatic reactions were performed at 30°C in mixed solutions containing 0.3 μM Pyrl4 or its variant, 50 mM Tris-HCl buffer (pH 7.0) and varying concentrations of **1** (0, 25, 50, 100, 200, 400, 600, or 800 μM). All assays were performed in triplicate. The resulting initial velocities were fitted to the Michaelis-Menten equation using OriginPro 8 (Originlab) to extract the parameters K_m and k_{cat}.

In Situ NMR Monitoring of the Enzymatic Conversion of Substrate 1 to Product 2

Compound **1** (2 mM) was dissolved in the CD_3OD/D_2O mixture (52%, v/v). The reaction was initiated by the addition of Pyrl4 or the variant Pyrl4-Δ10 to a final concentration of 2 μM and then monitored over an 800-min period at 25°C on an Agilent 800 MHz spectrometer equipped with a cryogenic probe (Agilent Technologies). The reaction proceeding in the absence of the enzyme was used as a negative control.

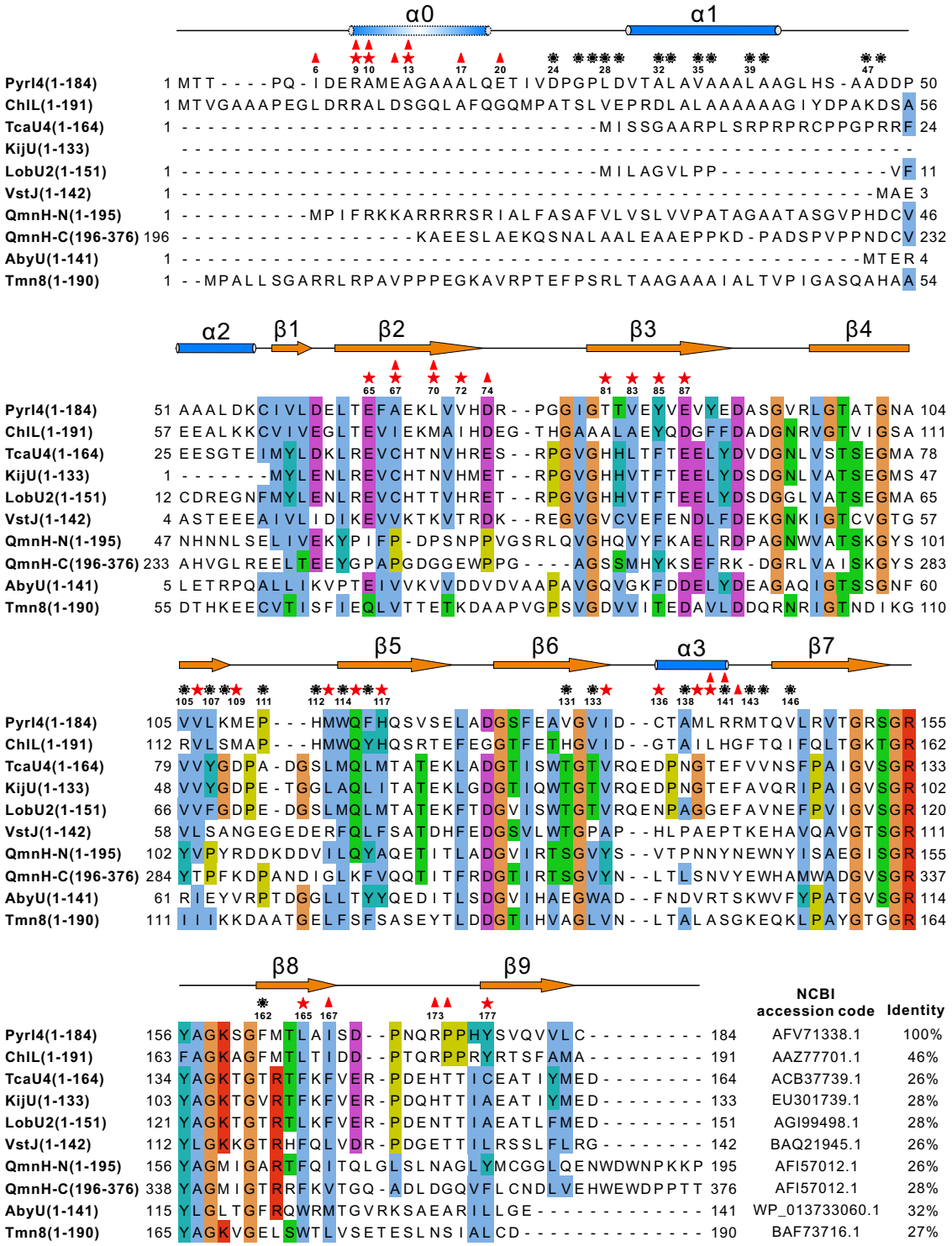

Figure 6. Structure-Based Sequence Alignment of Pyrl4 to Its Homologs and their Associated Spiro-Conjugate Moieties in the Corresponding Natural Products

The conserved residues are highlighted in color using Jalview2.8.1 software (http://www.jalview.org/). The residues of Pyrl4 that are involved in the dimer interface are highlighted with black asterisks. The residues that are important for the interactions between Pyrl4 and the ligand and between the β barrel and the N-terminal sequence are highlighted with red stars and red triangles, respectively. The associated accession codes in the NCBI database and sequence identities with Pyrl4 are also included for all the homologs.

NMR Analysis of Pyrl4 and Its Variant Pyrl4-Δ10

The protein samples for NMR analyses were concentrated to ~0.2 mM (for titration experiments) or ~1.0 mM (for backbone resonance assignment) in 50 mM potassium phosphate buffer (pH 6.5) containing 50 mM NaCl, 1 mM DTT, and 1 mM EDTA. The transverse relaxation optimized spectroscopy version of the ^{1}H-^{15}N HSQC spectra were acquired at 35°C on an Agilent 800 MHz spectrometer equipped with a cryogenic probe (Agilent Technologies). All NMR data were processed with NMRPipe (Delaglio et al., 1995). Backbone resonance assignment of the N-terminal 22 residues was achieved by the combination of several standard heteronuclear correlation experiments (Wuthrich, 1986; Bax and Grzesiek, 1993).

Molecular Simulation

Docking of ligand **1** into Pyrl4 was performed using Maestro v9.0 (Schrödinger, 2011; Friesner et al., 2004). First, **1** was processed with the LigPrep (Schrödinger, 2011) module to produce the corresponding low-energy three-dimensional structure and the correct ionization state (pH 7.0). This process resulted in three ionization state structures, each of which has one negative charge, likely due to the low p*K*a value of **1** because of the presence of a tetramate moiety. Among them, only the structure that could be neutralized in the highly acidic β barrel core of Pyrl4 was chosen for docking. Next, the structure of Pyrl4 that forms the complex with ligand **2** was processed with the Protein Preparation Wizard module in Maestro to prepare the receptor structure. Water molecules within 4 Å from **2** were considered, and hydrogen atoms and protein charges were added over a brief relaxation period. Restrained partial minimization was conducted until the root-mean-square deviation reached a maximum value of 0.30 Å. The receptor-grid file was generated using an enclosing box centered on ligand **2** in the crystal structure with the default size. Then, **1** processed as described above was docked into the active site of Pyrl4 with Glide-XP (extra-precision) mode to output the top 20 conformations. Default settings were used for the refinement and scoring. The most reliable binding pose was selected according to the favorable interaction energy, similarity to the co-crystallized orientation of **2** in the complex structure, and our visual inspection from the conserved docking poses.

ACCESSION NUMBERS

Atomic coordinates and structural factors for the reported crystal structures are deposited in the PDB under accession numbers PDB: 5BTU and 5BU3.

SUPPLEMENTAL INFORMATION

Supplemental Information includes six figures and four tables and can be found with this article online at http://dx.doi.org/10.1016/j.chembiol.2016.01.005.

AUTHOR CONTRIBUTIONS

Y.G., Q.Z., L.P., J.L., and X.C. conducted structural investigations. Q.Z., Z.W., H.Z., and J.W. provided in vitro biochemical data. Q.Z., L.Y., Z.Z., H.Y. and H.J. performed theoretical studies. Q.Z., Y.G., L.P., and W.L. analyzed the data and wrote the manuscript. L.P. and W.L. directed the research.

ACKNOWLEDGMENTS

We thank SSRF BL17U and NCPSS BL19U1 for X-ray beam time, and Dr. Cong Liu for help with the MALS measurement. This work was supported in part by grants from MST (2013CB836900), Thousand Talents Program, STCSM (15JC1400400), and SRSSA (13QA1404300) of China (for L.P.); a grant from NSFC (91313000) of China (for H.J.); and grants from NSFC (31430005 and 21520102004), STCSM (14JC1407700 and 15JC1400400), and MST (2012AA02A706) of China (for W.L.); and a grant from NSFC (31300064) of China (for J.W.).

Received: December 14, 2015
Revised: January 13, 2016
Accepted: January 17, 2016
Published: February 11, 2016

REFERENCES

Adams, P.D., Grosse-Kunstleve, R.W., Hung, L.W., Ioerger, T.R., McCoy, A.J., Moriarty, N.W., Read, R.J., Sacchettini, J.C., Sauter, N.K., and Terwilliger, T.C. (2002). PHENIX: building new software for automated crystallographic structure determination. Acta Crystallogr. D Biol. Crystallogr. *58*, 1948–1954.

Bax, A., and Grzesiek, S. (1993). Methodological advances in protein NMR. Acc. Chem. Res. *26*, 131–138.

Davis, I.W., Leaver-Fay, A., Chen, V.B., Block, J.N., Kapral, G.J., Wang, X., Murray, L.W., Arendall, W.B., 3rd, Snoeyink, J., Richardson, J.S., et al. (2007). MolProbity: all-atom contacts and structure validation for proteins and nucleic acids. Nucleic Acids Res. *35*, W375–W383.

Delaglio, F., Grzesiek, S., Vuister, G.W., Zhu, G., Pfeifer, J., and Bax, A. (1995). NMRPipe-a multidimensional spectral processing system based on UNIX pipes. J. Biomol. NMR *6*, 277–293.

Ding, W., Williams, D.R., Northcote, P., Siegel, M.M., Tsao, R., Ashcroft, J., Morton, G.O., Alluri, M., Abbanat, D., Maiese, W.M., et al. (1994). Pyrroindomycins, novel antibiotics produced by *Streptomyces rugosporus* sp. LL-42D005. I. Isolation and structure determination. J. Antibiot. *47*, 1250–1257.

Du, H., and Ding, K. (2010). Asymmetric catalysis of Diels-Alder reaction. In Handbook of Cyclization Reactions, S. Ma, ed. (Wiley-VCH Verlag), pp. 1–57.

Emsley, P., and Cowtan, K. (2004). Coot: model-building tools for molecular graphics. Acta Crystallogr. D Biol. Crystallogr. *60*, 2126–2132.

Fage, C.D., Isiorho, E.A., Liu, Y., Wagner, D.T., Liu, H.-w., and Keatinge-Clay, A.T. (2015). The structure of SpnF, a standalone enzyme that catalyzes [4+2] cycloaddition. Nat. Chem. Biol. *11*, 256–258.

Friesner, R.A., Banks, J.L., Murphy, R.B., Halgren, T.A., Klicic, J.J., Mainz, D.T., Repasky, M.P., Knoll, E.H., Shelley, M., Perry, J.K., et al. (2004). Glide: a new approach for rapid, accurate docking and scoring. 1. Method and assessment of docking accuracy. J. Med. Chem. *47*, 1739–1749.

Gouverneur, V.E., Houk, K.N., de Pascual-Teresa, B., Beno, B., Janda, K.D., and Lerner, R.A. (1993). Control of the exo and endo pathways of the Diels-Alder reaction by antibody catalysis. Science *262*, 204–208.

Green, M.R., and Sambrook, J. (2012). Molecular Cloning: a Laboratory Manual, Fourth Edition (Cold Spring Harbor Laboratory Press).

Hashimoto, T., Hashimoto, J., Teruya, K., Hirano, T., Shin-ya, K., Ikeda, H., Liu, H.-w., Nishiyama, M., and Kuzuyama, T. (2015). Biosynthesis of versipelostatin: identification of an enzyme-catalyzed [4+2]-cycloaddition required for macrocyclization of spirotetronate-containing polyketides. J. Am. Chem. Soc. *137*, 572–575.

Jia, X., Tian, Z., Shao, L., Qu, X., Zhao, Q., Tang, J., Tang, G., and Liu, W. (2006). Genetic characterization of the chlorothricin gene cluster as a model for spirotetronate antibiotic biosynthesis. Chem. Biol. *13*, 575–585.

Kim, H.J., Ruszczycky, M.W., Choi, S.H., Liu, Y.N., and Liu, H.-W. (2011). Enzyme-catalysed [4+2] cycloaddition is a key step in the biosynthesis of spinosyn A. Nature *473*, 109–112.

Kim, H.J., Ruszczycky, M.W., and Liu, H.-W. (2012). Current developments and challenges in the search for a naturally selected Diels-Alderase. Curr. Opin. Chem. Biol. *16*, 124–131.

Klas, K., Tsukamoto, S., Sherman, D.H., and Williams, R.M. (2015). Natural Diels-Alderases: elusive and irresistible. J. Org. Chem. *80*, 11672–11685.

Lacoske, M.H., and Theodorakis, E.A. (2015). Spirotetronate polyketides as leads in drug discovery. J. Nat. Prod. *78*, 562–575.

Murshudov, G.N., Vagin, A.A., and Dodson, E.J. (1997). Refinement of macromolecular structures by the maximum-likelihood method. Acta Crystallogr. D Biol. Crystallogr. *53*, 240–255.

Neumann, P., Brodhun, F., Sauer, K., Herrfurth, C., Hamberg, M., Brinkmann, J., Scholz, J., Dickmanns, A., Feussner, I., and Ficner, R. (2012). Crystal structures of *Physcomitrella patens* AOC1 and AOC2: insights into the enzyme mechanism and differences in substrate specificity. Plant Physiol. *160*, 1251–1266.

Oikawa, H., and Tokiwano, T. (2004). Enzymatic catalysis of the Diels-Alder reaction in the biosynthesis of natural products. Nat. Prod. Rep. *21*, 321–352.

Otwinowski, Z., and Minor, W. (1997). Processing of X-ray diffraction data collected in oscillation mode. Methods Enzymol. *276*, 307–326.

Pang, B., Wang, M., and Liu, W. (2016). Cyclization of polyketides and non-ribosomal peptides on and off their assembly lines. Nat. Prod. Rep. http://dx.doi.org/10.1039/C5NP00095E.

Schrödinger. (2011). LigPrep, Version 2.5 (Schrödinger LLC).

Seelig, B., and Jäschke, A. (1999). A small catalytic RNA motif with Diels-Alderase activity. Chem. Biol. *6*, 167–176.

Siegel, J.B., Zanghellini, A., Lovick, H.M., Kiss, G., Lambert, A.R., St Clair, J.L., Gallaher, J.L., Hilvert, D., Gelb, M.H., Stoddard, B.L., et al. (2010). Computational design of an enzyme catalyst for a stereoselective bimolecular Diels-Alder reaction. Science *329*, 309–313.

Singh, M.P., Petersen, P.J., Jacobus, N.V., Mroczenski-Wildey, M.J., Maiese, W.M., Greenstein, M., and Steinberg, D.A. (1994). Pyrroindomycins, novel antibiotics produced by *Streptomyces rugosporus* LL-42D005. II. Biological activities. J. Antibiot. *47*, 1258–1265.

Storoni, L.C., McCoy, A.J., and Read, R.J. (2004). Likelihood-enhanced fast rotation functions. Acta Crystallogr. D Biol. Crystallogr. *60*, 432–438.

Terwilliger, T.C., Adams, P.D., Read, R.J., McCoy, A.J., Moriarty, N.W., Grosse-Kunstleve, R.W., Afonine, P.V., Zwart, P.H., and Hung, L.W. (2009). Decision-making in structure solution using Bayesian estimates of map quality: the PHENIX AutoSol wizard. Acta Crystallogr. D Biol. Crystallogr. *65*, 582–601.

Tian, Z., Sun, P., Yan, Y., Wu, Z., Zheng, Q., Zhou, S., Zhang, H., Yu, F., Jia, X., Chen, D., et al. (2015). An enzymatic [4+2] cyclization cascade creates the pentacyclic core of pyrroindomycins. Nat. Chem. Biol. *11*, 259–265.

Wu, Q., Wu, Z., Qu, X., and Liu, W. (2012). Insights into pyrroindomycin biosynthesis reveal a uniform paradigm for tetramate/tetronate formation. J. Am. Chem. Soc. *134*, 17342–17345.

Wuthrich, K. (1986). NMR of Proteins and Nucleic Acids (Wiley-Interscience).

Yamaguchi, T., Saito, K., Tsujimoto, T., and Yuki, H. (1976). NMR spectroscopic studies on the tautomerism in tenuazonic acid analogs. J. Heterocycl. Chem. *13*, 533–537.

Zheng, Q., Tian, Z., and Liu, W. (2016). Recent advances in understanding the enzymatic reactions of [4+2] cycloaddition and spiroketalization. Curr. Opin. Chem. Biol. *31*, http://dx.doi.org/10.1016/j.cbpa.2016.01.020.

Cell Chemical Biology, Volume *23*

Supplemental Information

Enzyme-Dependent [4 + 2] Cycloaddition Depends on Lid-like Interaction of the N-Terminal Sequence with the Catalytic Core in Pyrl4

Qingfei Zheng, Yujiao Guo, Linlin Yang, Zhixiong Zhao, Zhuhua Wu, Hua Zhang, Jianping Liu, Xiaofang Cheng, Jiequn Wu, Huaiyu Yang, Hualiang Jiang, Lifeng Pan, and Wen Liu

Supporting Information

Enzyme-Dependent [4 + 2] Cycloaddition Depends on Lid-like Interaction of the N-Terminal Sequence with the Catalytic Core in PyrI4

Qingfei Zheng[1,4], Yujiao Guo[1,4], Linlin Yang[2], Zhixiong Zhao[1], Zhuhua Wu[1], Hua Zhang[1], Jianping Liu[1], Xiaofang Cheng[1], Jiequn Wu[1,3], Huaiyu Yang[2], Hualiang Jiang[2], Lifeng Pan[1,*], and Wen Liu[1,3,**]

[1] State Key Laboratory of Bioorganic and Natural Products Chemistry, Shanghai Institute of Organic Chemistry, Chinese Academy of Sciences, 345 Lingling Road, Shanghai 200032, China

[2] Drug Discovery and Design Center, State Key Laboratory of Drug Research, Shanghai Institute of Materia Medica, Chinese Academy of Sciences, 555 Zu-Chong-Zhi Road, Shanghai 201203, China

[3] Huzhou Center of Bio-Synthetic Innovation, 1366 Hongfeng Road, Huzhou 313000, China

[4] Co-first author

*Correspondence: panlf@sioc.ac.cn

**Correspondence: wliu@mail.sioc.ac.cn

Supplementary Figures

Figure S1. Charaterization of the dimeric nature of PyrI4 in solution (related to Figure 2)

Figure S2. NMR analysis of the *N*-terminal sequence (residues 1-22) of PyrI4 (related to Figures 2, 3, 4 and 5)

Figure S3. Detailed structural analysis of PyrI4 and its complex with **2** (related to Figures 2, 3 and 4)

Figure S4. Three-dimensional homologs of PyrI4 (related to Figure 2)

Figure S5. *In situ* NMR monitoring of the enzymatic conversion of substrate **1** into product **2** (related to Figures 1, 2, 3, 4 and 5)

Figure S6. Analysis of PyrI4 in solution by NMR (related to Figures 2, 3, 4and 5)

Supplementary Tables

Table S1. Protein Crystal Data (related to Figure 2)

Table S2. Kinetic Analysis Data (related to Figure 4)

Table S3. Bacterial Strains and Plasmids (related to Figures 2, 3, 4 and 5)

Table S4. Primers Used in This Study (related to Figures 2, 3, 4 and 5)

Supplementary References

Supplementary Figures

Figure S1 (related to Figure 2). Characterization of the dimeric nature of PyrI4 in solution. **A**, Coomassie blue-stained SDS-PAGE analysis showing the purified PyrI4 and mono-ubiquitin before and after lysine-specific cross-linking with DSG. **B**, Multiangle light scattering (MALS) analysis of PyrI4 (residues 1–184), showing the relative light scattering signal as a function of elution volume. The derived molecular mass of the peak is shown in blue.

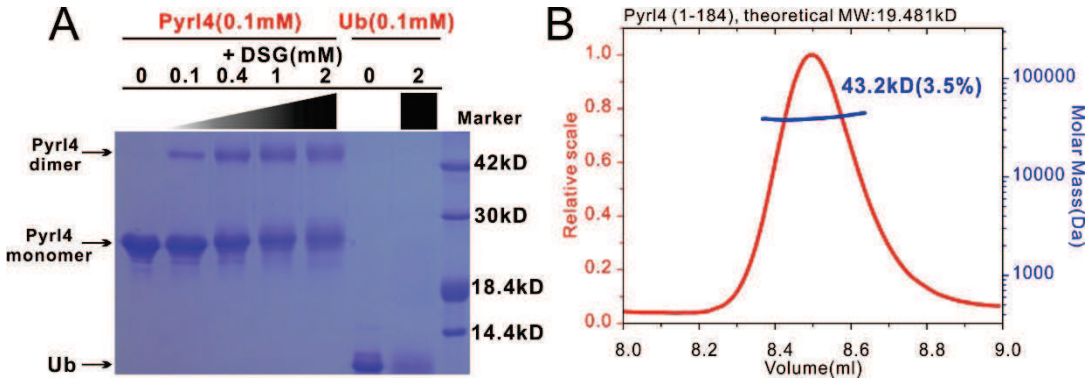

Figure S2 (related to Figures 2, 3, 4 and 5). NMR analysis of the *N*-terminal sequence (residues 1-22) of PyrI4. **A**, Overlay plot of the ^{1}H-^{15}N HSQC spectra of PyrI4 at two different contour levels. The labeled peaks corresponding to the *N*-terminal sequence (residues 1-22) are visible even at very high contour level (52000), indicating the flexible nature of this sequence. **B**, Assignments of the backbone chemical shifts of the *N*-terminal sequence based on the sequential HNCACB strips of 22 amino acid residues. **C**, Secondary chemical shifts of the *N*-terminal sequence (residues 1-22). The figure plots the combined C_α/C_β secondary chemical shifts as a function of amino acid residues. The secondary chemical shift, Δppm, of each residue is defined as $\Delta ppm = (^{13}C_{\alpha,exp}-^{13}C_{\alpha,rc}) - (^{13}C_{\beta,exp}-^{13}C_{\beta,rc})$, where $^{13}C_{\alpha,exp}$ and $^{13}C_{\beta,exp}$ are experimental chemical shifts of $^{13}C_\alpha$ and $^{13}C_\beta$, respectively, and $^{13}C_{\alpha,rc}$ and $^{13}C_{\beta,rc}$ are random coil chemical shifts for each residue. Each data point was smoothened by averaging the secondary chemical shifts of one residue immediately before and after a given amino acid. The amino acid sequence is also included at the top of the figure.

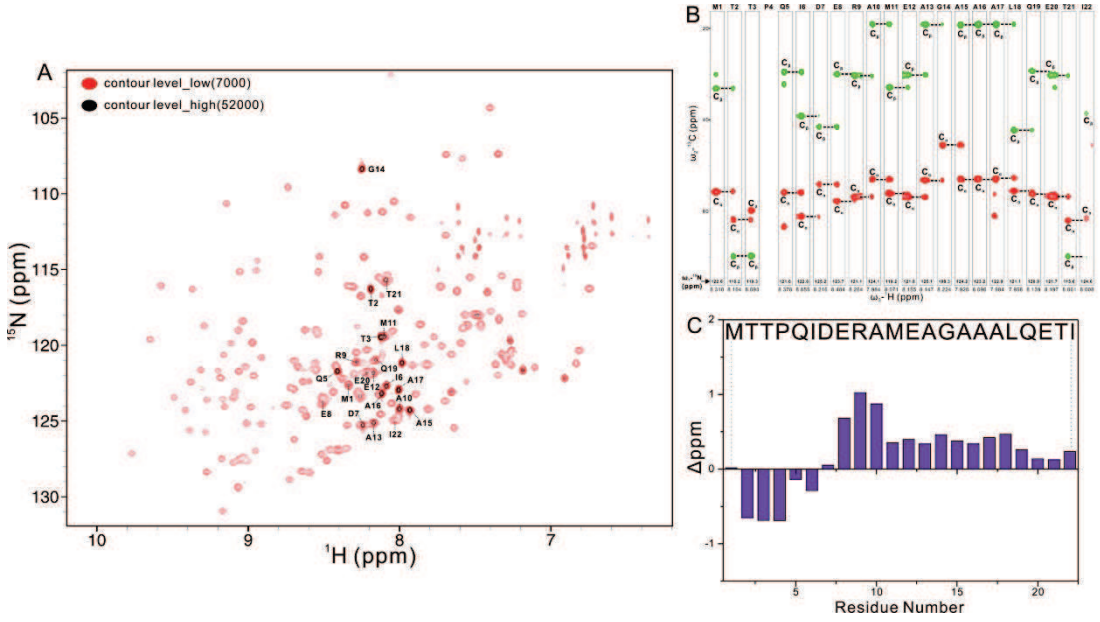

Figure S3 (related to Figures 2, 3 and 4). Detailed structural analysis of PyrI4 and its complex with **2**. **A**, Combination of ribbon representation and stick model showing the overall dimer interface. The two symmetrical inter-molecular binding sites mainly mediated by the α1-helix are formed by both extensive hydrophobic contacts and polar interactions. **B**, Combination of surface representation and the ribbon-stick model showing the hydrophobic interaction interface between two protein units. The hydrophobic amino acid residues in the surface model are drawn in yellow, the positively charged residues in blue, the negatively charged residues in red, and the uncharged polar residues in grey. **C**, Stereo view showing the detailed interactions of a symmetrical inter-molecular binding site between two protein units. The salt bridges and hydrogen bonds involved in the binding are shown as dotted lines. **c**, Enlarged portion for ligand binding. **D**, Combination of ribbon representation and stick-ball model for comparison of the conformations of the apo-protein (orange) and the complex (blue).

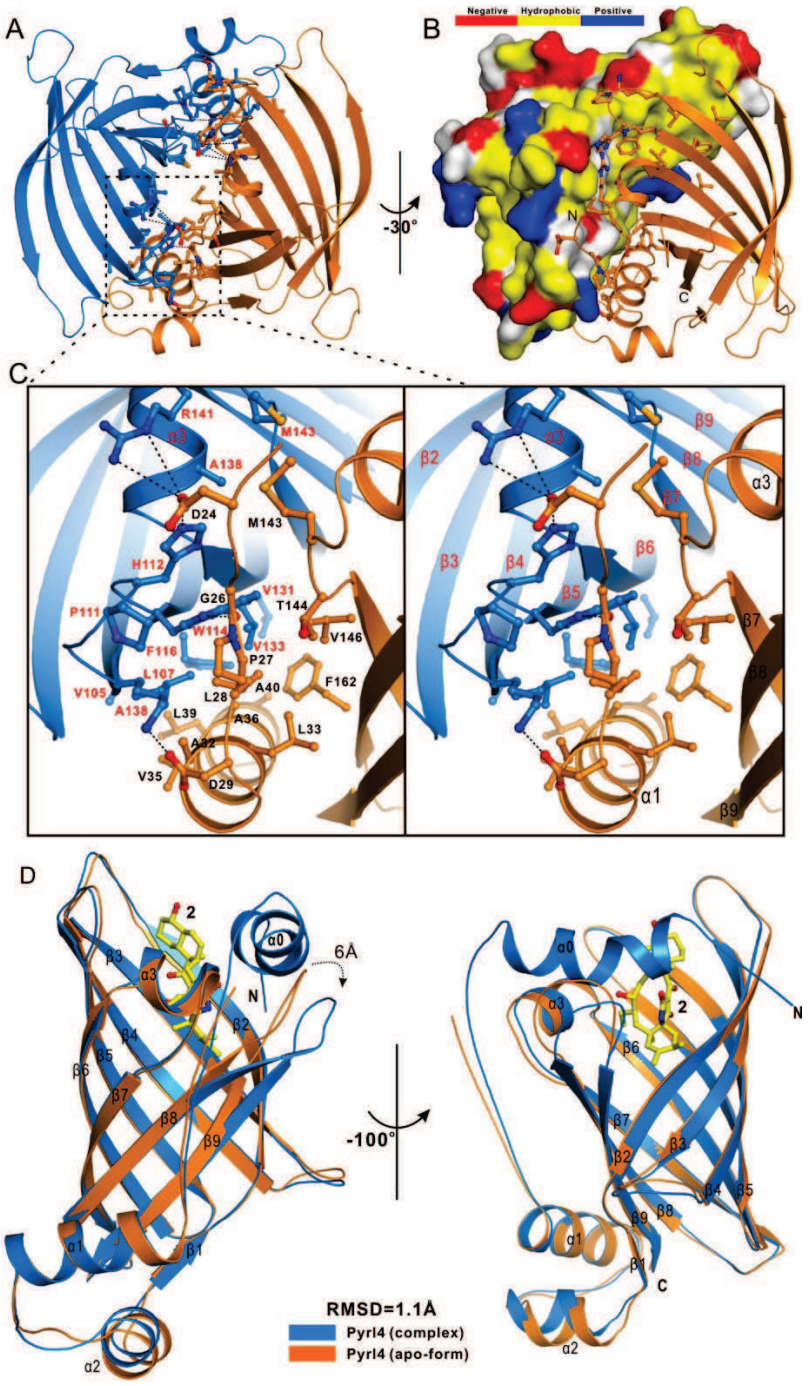
A
B
Negative
Hydrophobic
Positive
-30°
N
C
C
R141
α3
M143
A138
D24
M143
H112
G26
V131
T144
P111
W114
V146
F116
V133
P27
L107
A40
F162
V105
L28
A138
L39
A36
L33
A32
V35
D29
β2
α3
β9
β8
α3
β7
β3
β4
β6
β5
β7
β8
α1
β9
D
2
α0
6Å
β3
α3
N
β2
β4
β5
β6
β7
β8
β9
α1
β1
α2
-100°
α0
α3
2
N
β6
β7
β2
β3
β4
β5
β9
β8
α1
β1
C
α2
RMSD=1.1Å
Pyrl4 (complex)
Pyrl4 (apo-form)

Figure S4 (related to Figure 2). Three-dimensional homologs of PyrI4 that possess the similar monomeric β-barrel structures but different overall oligomeric architectures: YP583039.1 (**A** and **B**) and AOC (**C** and **D**).

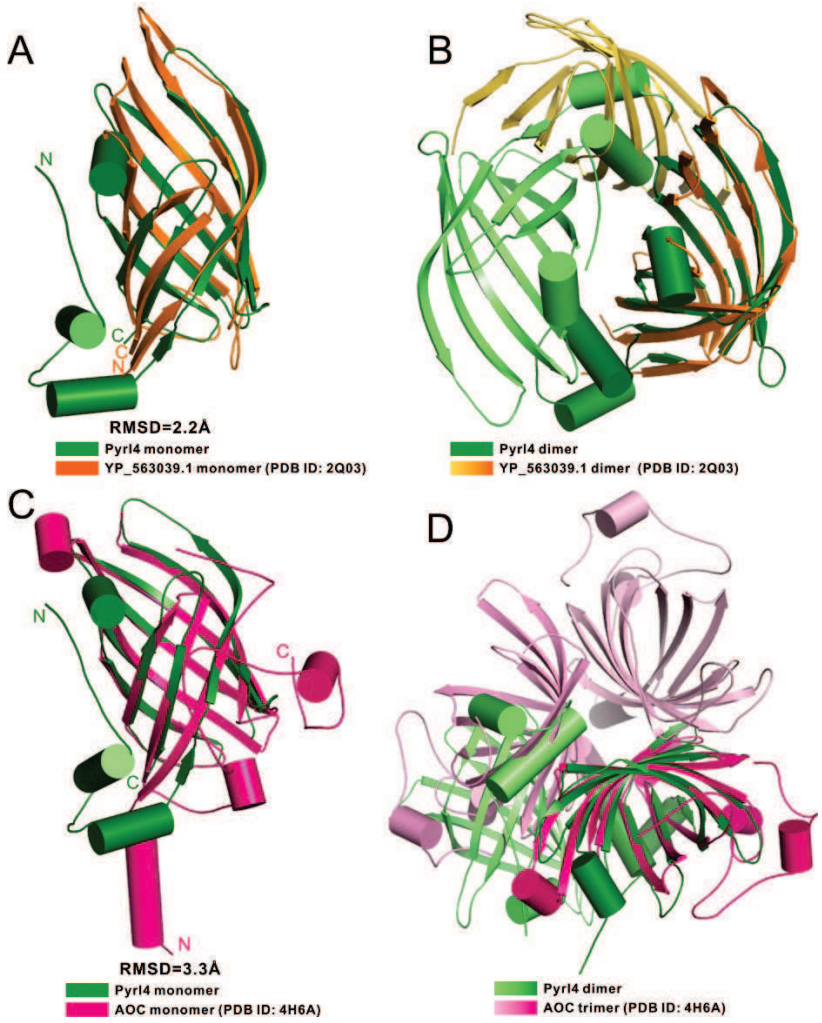

Figure S5 (related to Figures 1, 2, 3, 4 and 5). In situ NMR monitoring of the enzymatic conversion of substrate **1** into product **2**. The ^{1}H-NMR spectrum of **1** alone was used as a control. The NMR peaks corresponding to the hydrogens characteristic to substrate **1** and product **2** (referred to **Figure 1B**) are labeled in black and in red, respectively. **A**, Stack view of the partial ^{1}H-NMR spectra during the conversion process, in the presence of PyrI4 (with the molar ratio 1 : 1000 to 1). **B** and **C**, Stack view of the partial ^{1}H-NMR spectra, in the absence of PyrI4 and in the presence of the PyrI4-△10 variant (with the molar ratio 1 : 1000 to 1), respectively.

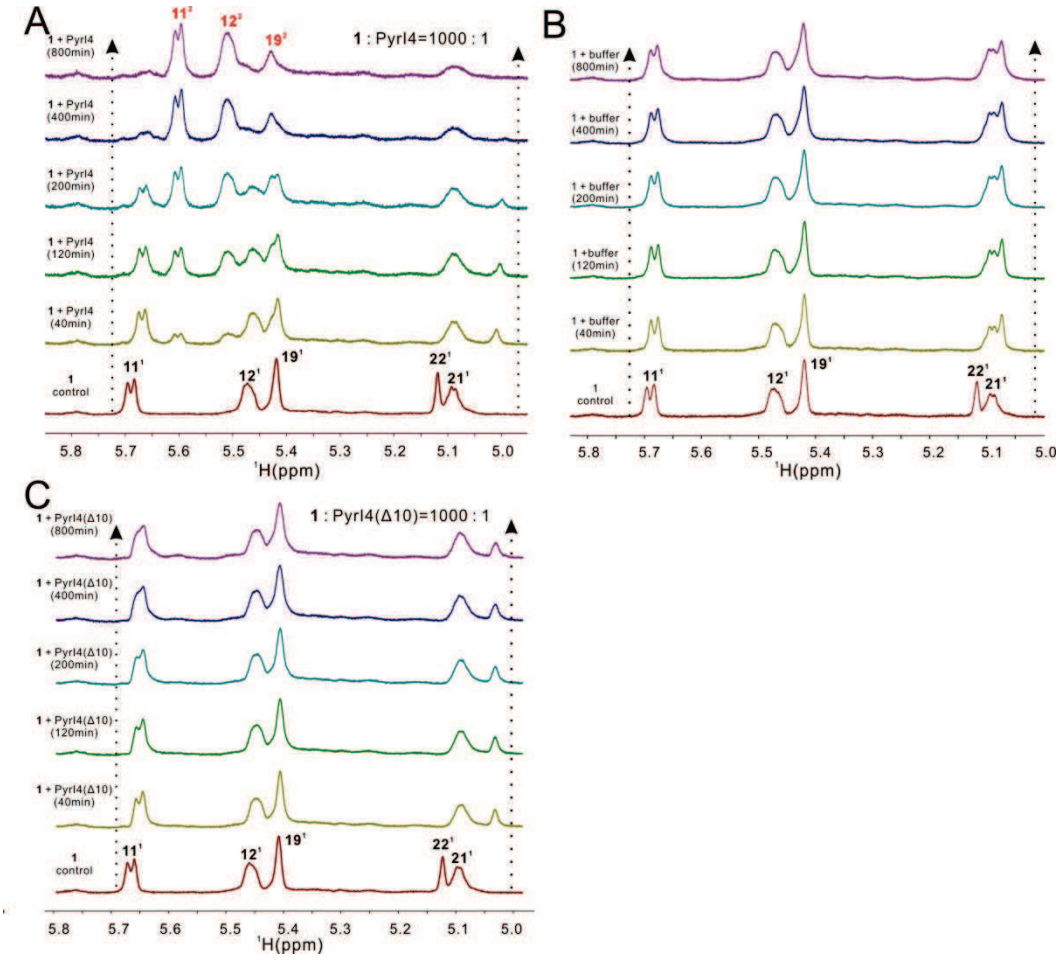

Figure S6 (related to Figures 2, 3, 4and 5). Analysis of PyrI4 in solution by NMR. **A**, Superposition plot of the ^{1}H-^{15}N HSQC spectra of PyrI4 in the titration with variable molar ratios of substrate **2** (dissolved in methanol). **B**, Overlay plot of the ^{1}H-^{15}N HSQC spectrum of PyrI4 (red) and PyrI4 in the presence of the same amount of methanol as in panel **a** (blue).

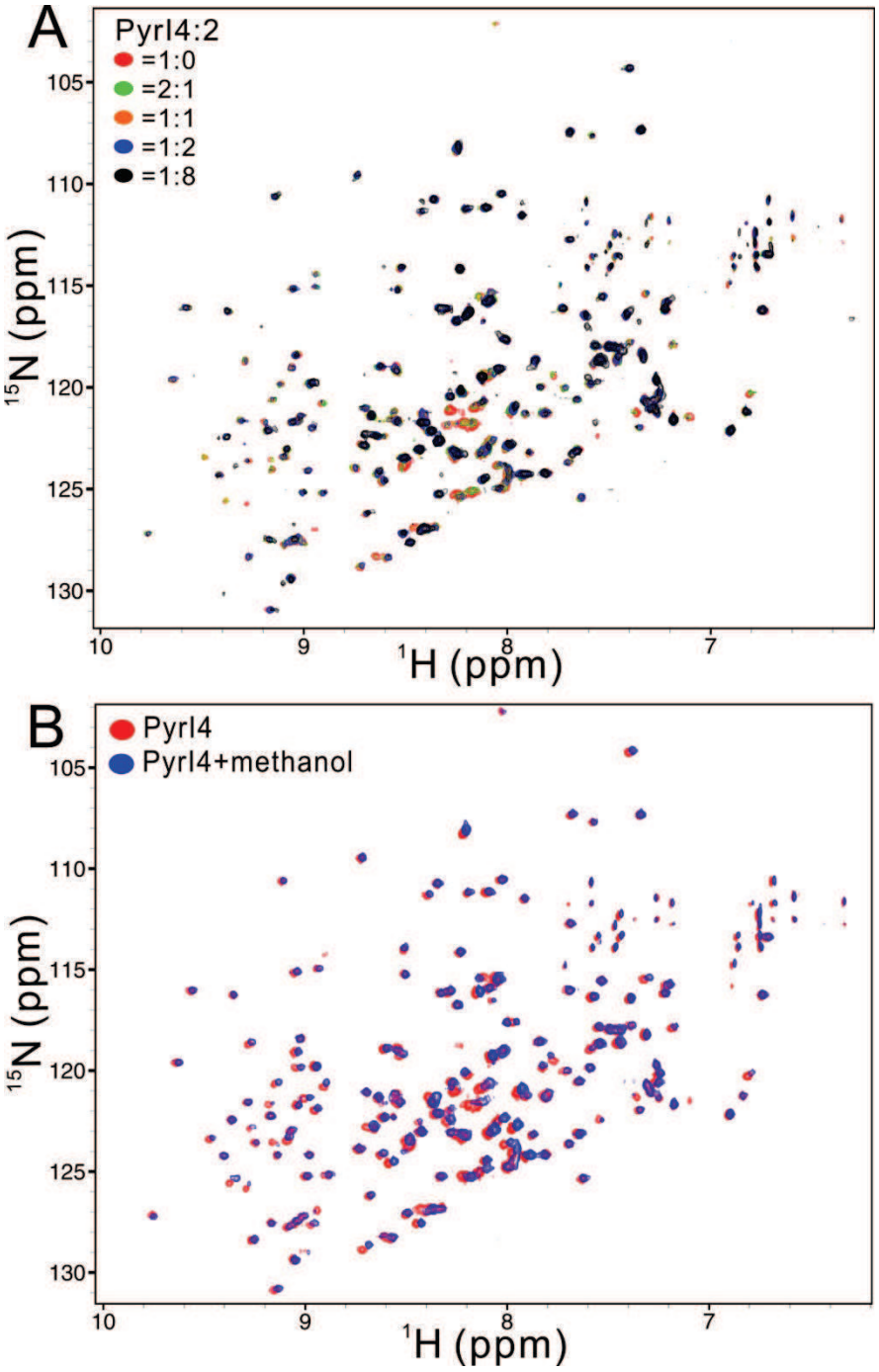

Supplementary Tables

Table S1 (related to Figure 2). Statistics of X-ray crystallographic data collection and model refinements.

	SeMet-PyrI4	PyrI4-**2** complex
Data collection		
Wavelength (Å)	0.9791	0.9785
Space group	P 32	P 21 21 21
Cell dimensions		
a, b, c (Å)	47.38, 47.38, 131.21	77.12, 91.03, 112.88
α, β, γ (°)	90, 90, 120	90, 90, 90
Resolution range (Å)	50.00 - 2.50 (2.54 - 2.50)	50.00 - 1.90 (1.93 - 1.90)
R_{merge} (%)[a]	0.091 (0.969)	0.105 (0.890)
Mean I/sigma(I)	43.45 (7.62)	17.03 (4.54)
Completeness (%)	99.7 (100.0)	99.9 (99.9)
Redundancy	10.6 (10.1)	11.6 (11.3)
Structure refinement		
Resolution (Å)	39.16 - 2.50 (2.75 - 2.50)	39.20 - 1.90 (1.93 - 1.90)
R_{cryst} / R_{free} (%)[b]	18.21 (25.43) / 24.99 (40.10)	17.28 (23.74) / 20.66 (27.94)
r.m.s.d bonds (Å) / angles (°)	0.009 / 1.17	0.012 / 1.90
Average B-factor (Å^2)	87.4	22.2
No. of atoms		
macromolecules	2387	5372
ligands	48	192
water	10	718
Ramachandran plot[c]		
favored region (%)	95.00	98.0
allowed region (%)	4.69	2.0
outliers (%)	0.31	0

[a] $R_{merge} = \sum|I_i - I_m|/\sum I_i$, where I_i is the intensity of the measured reflection and Im is the mean intensity of all symmetry related reflections.

[b] $R_{cryst} = \Sigma||F_{obs}| - |F_{calc}||/\Sigma|F_{obs}|$, where F_{obs} and F_{calc} are observed and calculated structure factors. $R_{free} = \Sigma_T||F_{obs}| - |F_{calc}||/\Sigma_T|F_{obs}|$, where T is a test data set of about 5% of the total reflections randomly chosen and set aside prior to refinement.

[c] Defined by Molprobity.

Numbers in parentheses represent the value for the highest resolution shell.

Table S2 (related to Figure 4). Steady-state kinetic parameters of the enzymatic [4+2] cycloaddition reaction catalyzed by PyrI4 or its variant.

Mutant protein	K_m (μM)	k_{cat} (min^{-1})	k_{cat}/K_m (μM^{-1} min^{-1})
PyrI4-WT	224.0 ± 3.5	342.6 ± 3.3	1.5
PyrI4-Q115A	289.4 ± 26.4	104.3 ± 3.9	0.36
PyrI4-Y85A	233.5 ± 22.4	228.3 ± 8.2	0.98
PyrI4-E87A	234.8 ± 17.8	288.7 ± 8.2	1.2
PyrI4-E65A	228.0 ± 24.6	222.2 ± 8.9	0.97
PyrI4-Y177A	226.0 ± 11.9	324.3 ± 6.3	1.4
PyrI4-H117A	239.8 ± 14.3	325.2 ± 7.3	1.4

Table S3 (related to Figures 2, 3, 4 and 5). Bacterial strains and plasmids.

Strain/Plasmid	Characteristic(s)	Source/Reference
E.coli		
DH5α	Host for general cloning	Invitrogen
BL21 (DE3)	Host for protein expression	NEB
Plasmids		
pWL1024	pET-28a(+) derivative, for expressing PyrI4 in a 6 × His-tagged form	1
pWL2000	pWL1024 derivative, for mutation of Q115A in PyrI4	This study
pWL2001	pWL1024 derivative, for mutation of E65A in PyrI4	This study
pWL2002	pWL1024 derivative, for mutation of E87A in PyrI4	This study
pWL2003	pWL1024 derivative, for mutation of Y85A in PyrI4	This study
pWL2004	pWL1024 derivative, for mutation of H117A in PyrI4	This study
pWL2005	pWL1024 derivative, for mutation of I134A in PyrI4	This study
pWL2006	pWL1024 derivative, for mutation of M139A in PyrI4	This study
pWL2007	pWL1024 derivative, for mutation of Y177A in PyrI4	This study
pWL2008	pWL1024 derivative, for mutation of Q115/Y85A in PyrI4	This study
pWL2009	pWL1024 derivative, for mutation of Q115/Y85A/E65A in PyrI4	This study

pWL2010	pWL1024 derivative, for mutation of Q115/Y85A/E65A/E87A in PyrI4	This study
pWL2011	pWL1024 derivative, for mutation of Y85A/E65A/E87A in PyrI4	This study
pWL2012	pWL1024 derivative, for mutation of Y85A/E65A/E87A/Y117A in PyrI4	This study
pWL2013	pWL1024 derivative, for mutation of E20R in PyrI4	This study
pWL2014	pWL1024 derivative, for mutation of D74R in PyrI4	This study
pWL2015	pWL1024 derivative, for mutation of R9A in PyrI4	This study
pWL2016	pWL1024 derivative, for expressing the PyrI4-△10 variant in which the 1-10-aa *N*-terminal sequence of PyrI4 was deleted	This study

Table S4 (related to Figures 2, 3, 4 and 5). Primers Used in This Study. The codons for site-specific mutation in PyrI4 are indicated in red.

Primer	Sequence
Q115A-for	5'- ATG GAG CCG CAC ATG TGG GCG TTC CAC CAG AGC GTC TCC -3'
Q115A-rev	5'- GGA GAC GCT CTG GTG GAA CGC CCA CAT GTG CGG CTC CAT -3'
E65A-for	5'- GTC CTG GAC GAG CTC ACC GCG TTC GCC GAG AAG CTC GTC -3'
E65A-rev	5'- GAC GAG CTT CTC GGC GAA CGC GGT GAG CTC GTC CAG GAC -3'
E87A-for	5'- ACC GTC GAG TAC GTC GCG GTC TAC GAG GAC -3'
E87A-rev	5'- GTC CTC GTA GAC CGC GAC GTA CTC GAC GGT -3'
Y85A-for	5'- ATC GGC ACC ACC GTC GAG GCG GTC GAG GTC TAC GAG GAC -3'
Y85A-rev	5'- GTC CTC GTA GAC CTC GAC CGC CTC GAC GGT GGT GCC GAT -3'
H117A-for	5'- ATG GAG CCG CAC ATG TGG CAG TTC GCC CAG AGC GTC TCC -3'
H117A-rev	5'- GGA GAC GCT CTG GGC GAA CTG CCA CAT GTG CGG CTC CAT -3'
I134A-for	5'- TTC GAG GCG GTC GGC GTC GCG GAC TGC ACG GCG ATG CTG -3'
I134A-rev	5'- CAG CAT CGC CGT GCA GTC CGC GAC GCC GAC CGC CTC GAA -3'
M139A-for	5'- ATC GAC TGC ACG GCG GCG CTG CGC CGG ATG ACC -3'
M139A-rev	5'- GGT CAT CCG GCG CAG CGC CGC CGT GCA GTC GAT -3'
Y177A-for	5'- CAG CGG CCT CCG CAC GCC TCG GTG CAA GTC -3'
Y177A-rev	5'- GAC TTG CAC CGA GGC GTG CGG AGG CCG CTG -3'
Δ10-for	5'- ATATCATATGGAAGCAGGCGCTGCCGCCCTCCAGG -3' (*Nde* I)
Δ10-rev	5'- ATATCTCGAGTCAGCAGAGGACGACTTGCACCGAG -3' (*Xho* I)

E20R-for	5’- GCT GCC GCC CTC CAG CGC ACG ATC GTG GAC CCG -3’
E20R-rev	5’- CGG GTC CAC GAT CGT GCG CTG GAG GGC GGC AGC -3’
D74R-for	5’- AAG CTC GTC GTC CAC CGC CGG CCC GGC GGC ATC -3’
D74R-rev	5’- GAT GCC GCC GGG CCG GCG GTG GAC GAC GAG CTT -3’
R9A-for	5’- ACC CCG CAG ATC GAC GAG GCG GCC ATG GAA GCA GGC GCT -3’
R9A-rev	5’- AGC GCC TGC TTC CAT GGC CGC CTC GTC GAT CTG CGG GGT -3’

Supplementary References

1. Tian, Z., Sun, P., Yan, Y., Wu, Z., Zheng, Q., Zhou, S., Zhang, H., Yu, F., Jia, X., Chen, D., et al. (2015) An enzymatic [4+2] cyclization cascade creates the pentacyclic core of pyrroindomycins. Nat. Chem. Biol. *11*, 259-265.